Progress In Electromagnetics Research C, Vol. 92, 239–250, 2019

A Dual-Band Planar Quasi Yagi-Uda Antenna with Optimized Gain for LTE Applications

Manzoor Elahi[1], Irfanullah[2], Rizwan Khan[3, 4, *], Azremi Abdullah Al-Hadi[3], Saeeda Usman[1], and Ping Jack Soh[3]

Abstract—A printed Yagi-Uda antenna with two closely-spaced driven dipole elements and truncated ground plane is presented for dual-band operation. It is designed on a low-cost FR4 substrate with a dielectric constant 4.6, loss tangent of 0.02, and thickness of 1.6 mm. The dipole, operating in the lower band (centered at 1.8 GHz), is elliptical-bow-tie in shape with rounded edges, whereas a J-shaped dipole enables its operation in the upper band (centered at 2.6 GHz). A trapezoid-shaped director is employed to achieve maximum gain over the required frequency bands. Measurements indicate that the antenna operates from 1.71 to 1.9 GHz and from 2.5 to 2.7 GHz with $|S_{11}| < -10$ dB. The behavior of the proposed antenna has been investigated by studying different parameters to achieve the maximum gains of 6 and 7.7 dB in LTE band 3 and band 7, respectively, with optimal size. It is found that the experimental results of the final packaged antenna agree with the simulated ones in terms of reflection coefficients, gain, and radiation patterns.

1. INTRODUCTION

The demand for higher data rates in modern wireless communication system is increasing rapidly. The advent of Long Term Evolution (LTE) enables long distance and high-speed data applications such as video and multimedia [1, 2]. Besides that, the problems of interference and multipath fading which degrades system performance can be reduced by employing sectoring and beam switching [3]. Therefore, an end-fire antenna which features a unidirectional main beam with high gain and directivity along the antenna length can be deployed. These end-fire antennas are suitable for airborne vehicle, such as aircrafts and missiles, facilitating the vehicle tracking on their ascent or descent. Presently these end-fire antennas are also employed in many other applications such as in point-to-point communication [4], personal area network [5], and for radar applications [6].

Conventional Yagi-Uda antenna has been investigated in the past several decades. Its gradual evolution resulted in the form of a quasi-Yagi antenna [7–10], a printed form of the classical Yagi-Uda with a smaller size and wider bandwidth. This antenna type is one of the preferred choices when a high gain and front-to-back ratio (FBR) is required. However, these antennas are limited in terms of gain, directivity, and FBR when size is considered.

To alleviate these limitations, several design approaches have been adopted. A single-band antenna operating from 1.8 to 2.4 GHz is proposed in [11]. The antenna is fed by a series of microstrip lines, with one printed on the same side and directly connected to one of the active branches of the dipole. The other line is printed on the reverse side of the substrate and is connected to another branch of the dipole

Received 24 February 2019, Accepted 12 May 2019, Scheduled 20 May 2019

* Corresponding author: Rizwan Khan (jadoon.rizwankhan57@gmail.com).

[1] Department of Electrical Engineering, COMSATS Institute of Information Technology, Sahiwal, Punjab, Pakistan. [2] Department of Electrical Engineering, COMSATS Institute of Information Technology, Abbottabad, K.P.K, Pakistan. [3] Advanced Communication Engineering (ACE) Centre of Excellence, School of Computer and Communication Engineering, Universiti Malaysia Perlis, Perlis, Malaysia. [4] Department of Research and Development, Laird Technologies (M) Sdn Bhd, Penang, Malaysia.

through a via hole. This resulted in a maximum gain of 6 dB at 2.4 GHz. The antenna presented in [12] uses the same feeding mechanism as [11]. A high gain of 7.5 dB at 2.5 GHz is achieved with parabolic reflector. However, the high gain is produced at the expense of its larger dimension ($0.996\lambda_g \times 1.687\lambda_g$). A single band compact design ($0.581\lambda_g \times 0.581\lambda_g$) in [13] operates between 1.9 and 2.5 GHz. Although the size is small, the gain and directivity of 5 and 5.5 dB, respectively, are also relatively low.

A high gain Yagi antenna is designed by using a split ring resonator (SRR) as its director [14], featuring a dual resonance mode with directivities of 5.7 and 6.3 dB at 3.45 and 5.2 GHz, respectively. This, however, also results in a larger dimension of $1.048\lambda_g \times 1.43\lambda_g$. Another approach is to use two parallel dipoles to facilitate the operation in two bands, which has been investigated in [15]. The antenna operates from 2.4 to 2.484 GHz with gains between 3.7 dB and 4.3 dB, and from 5.15 to 5.85 GHz with gains from 2.7 dB to 6 dB. Despite this, its size of $1.168\lambda_g \times 1.247\lambda_g$ is still considered large. Researchers in [16] present a miniaturized ($0.573\lambda_g \times 0.833\lambda_g$) dual-band antenna, operating from 1.45 to 2.55 GHz and from 3.707 to 4.71 GHz. Despite its small size, the gain and directivity are low, i.e., 4.23 and 4.33 dB in the lower and upper bands, respectively. To enable a dual-band characteristic and directional radiation in [17], a pair of multiple drivers along with multiple parasitic directors and reflector is used. The overall size of the antenna is $0.475\lambda_g \times 0.748\lambda_g$, with gain ranging from 4.1 dB to 5.8 dB in the two bands, i.e., from 2.39 to 2.51 GHz, and from 4.83 to 5.97 GHz.

Based on the topology in [17], triple band operation is enabled by multiple drivers, designed on the basis of a classical dipole configuration, with embedded L-shaped slotlines in [18]. The combination of branch line directors and a stepped impedance reflector are used, resulting in gains of 6.29, 4.63, and 6.77 dB, and FBRs of 11.8, 12.6, and 13.6 dB at 1.89, 2.54, and 3.51 GHz, respectively. It is worth noticing that the gain in the lower band (at 1.89 GHz) is improved, at the cost of a larger antenna dimension ($0.723\lambda_g \times 0.836\lambda_g$). In [19], a tri-band CPW antenna with three parallel dipoles, based on the same concept as in [15] is proposed. The antenna size is $0.585\lambda_g \times 0.702\lambda_g$ and operates from 1.85 to 2 GHz, from 2.25 to 3.05 GHz, and from 3.35 to 3.8 GHz bands, but results in very low directivities of 2.8, 3.5, and 5.1 dB, respectively.

Ref. [20] presents the design of a Yagi antenna for single element as well as an array based on a square spiral ring (SSR). For a single element, high gains of 10.6, 5.26, and 6.7 dB are achieved at 2.79, 3.86, and 4.01 GHz, respectively, at the cost of relatively larger dimension of $0.8\lambda_g \times 1.83\lambda_g$. This Yagi antenna initially operates in a single band as its first resonance, whereas additional resonances and high gains are resultant of the integration of the SSR element. The final array resonates at multiple frequencies with bandwidths from 2.38 to 2.51 GHz and from 2.92 to 3.36 GHz, with an overall size of $1.59\lambda_g \times 1.83\lambda_g$. Next, a Yagi antenna is proposed in [21] with multiple operating bands between 698

Table 1. Comparison of the proposed antenna with other quasi-Yagi antenna available in literature.

Ref.	Size (mm)	Gain (dB)	Dir. (dB)	FBR (dB)	Bands (GHz)
[11]	$0.847\lambda_g \times 0.435\lambda_g$	5–6	N/A	> 10	1.8–2.4
[12]	$0.996\lambda_g \times 1.687\lambda_g$	7.5	N/A	N/A	2.28–2.6
[13]	$0.581\lambda_g \times 0.581\lambda_g$	5	5.5	N/A	1.9–2.5
[14]	$1.048\lambda_g \times 1.43\lambda_g$	N/A	5.7, 6.3	N/A	3.45, 5–5.57
[15]	$1.168\lambda_g \times 1.247\lambda_g$	3.7–4.3, 2.7–6	N/A	10	2.4–2.484, 5.15–5.85
[16]	$0.573\lambda_g \times 0.833\lambda_g$	4.23	4.33	8.5	1.45–2.55, 3.707–4.71
[17]	$0.475\lambda_g \times 0.748\lambda_g$	4.1–5.8	N/A	11, 9	2.39–2.51, 4.83–5.97
[18]	$0.723\lambda_g \times 0.836\lambda_g$	6.29, 4.63, 6.77	N/A	11.8, 12.6, 13.6	1.89, 2.54, 3.51
[19]	$0.585\lambda_g \times 0.702\lambda_g$	N/A	2.8, 3.5, 5.1	10	1.85–2, 2.25–3.05, 3.35–3.8
[20]	$0.8\lambda_g \times 1.83\lambda_g$	10.6, 5.26, 6.7	N/A	N/A	2.79, 3.86, 4.01
[21]	$0.56\lambda_g \times 0.41\lambda_g$	0.3–4.4	N/A	N/A	0.698–0.960, 1.720–1.880, 2.400–2.484
This work	$0.664\lambda_g \times 0.691\lambda_g$	4.3–6, 3.7–7.7	6.96, 7.9	22, 18.4	1.71–1.9, 2.5–2.7

and 960 MHz, between 1.72 and 1.88 GHz, and between 2.40 and 2.484 GHz for the GSM, DCS, and WLAN applications, respectively. The absolute gain varies between 0.3 and 4.4 dBi, whereas its overall size is $0.56\lambda_g \times 0.41\lambda_g$. This antenna is considered relatively small in size, with low gain and directivity.

In this work, a dual-band compact planar quasi-Yagi antenna fed by a microstrip to co-planar-stripline (CPS) transition is proposed, based on the method proposed in [12, 14, 15]. This unique antenna features a stack of modified, closely spaced driven elements and a semi-trapezoidal director to enable the operation in two required bands, with 6 dB and 7.7 dB of gain, respectively. This is enabled by the integration of a truncated ground plane as its reflector. The antenna operates from 1.71 to 1.9 GHz and from 2.5 to 2.7 GHz, which covers the LTE band 3 and band 7. Besides that, the FBRs are 22 and 18.4 dB at their respective center frequencies. A comparison of the published literature in terms of gain, directivity, and FBR with the proposed work is summarized in Table 1. It can be seen that the proposed antenna features improved performance in terms of gain, directivity, and FBR, while maintaining its compact size of $0.664\lambda_g \times 0.691\lambda_g$ in comparison with the published works in the literature. Due to the high gain, directivity, and front-to-back ratio, the proposed design has wide applications in wireless communication and is a good choice to mount it on base station.

The organization of the paper is as follows. The design and analysis of the antenna structure will first be explained in Section 2, followed by a parametric study of the important antenna parameters in Section 3. The simulated and measured results will be discussed in Section 4 before the concluding remarks in Section 5.

2. ANTENNA DESIGN AND ANALYSIS

The proposed dual-band quasi-Yagi antenna of size $63 \times 67\,\text{mm}^2$ ($0.664\lambda_g \times 0.691\lambda_g$) is designed on a low cost FR4 substrate, with a relative dielectric constant $\varepsilon_r = 4.6$, loss tangent $\tan\delta = 0.02$, and thickness 1.6 mm, as shown in Figure 1. It consists of a microstrip-to-CPS transition, double driven dipoles, and a parasitic director placed on top of the substrate. A truncated ground plane with a dimension of $H_G \times L_S$ located on the bottom of the substrate is used as a reflector. The microstrip-to-CPS transition [22, 23] is used to feed the antenna. To transmit power from the 50 Ω port to the asymmetric T-junction, a quarter wave transformer with a characteristic impedance of Z_0 is used to match the port impedance

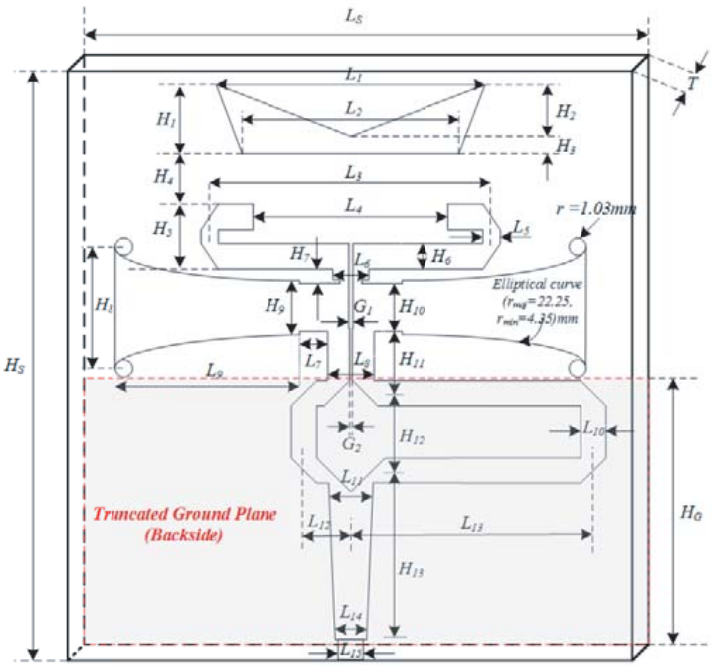

Figure 1. Geometry of the proposed quasi Yagi-Uda antenna.

to 25 Ω using Equation (1) [24]:

$$Z_0 = \sqrt{Z_L \times Z_{in}} \tag{1}$$

where Z_L and Z_{in} are the impedances at the two ends of the transformer. The characteristic impedance of the transformer, with a length of $H_{13} = \lambda_{gl}/4$, is 35.35 Ω. The width of transformer should be 4.9 mm based on [25], but this design incorporates width, tapering from L_{14} to L_{11} onto the transformer to obtain better impedance matching.

This is followed by an asymmetric T-junction which functions as a phase shifter, supplying 180° phase delay to generate the odd mode at 1.8 GHz. Thus, it transforms an unbalanced input signal to a balanced signal at the dipole element, resulting in radiation of the dipoles at their respective frequency bands from 1.71 to 1.9 GHz and from 2.5 to 2.7 GHz. This microstrip-to-CPS transition was initially designed for operation at 1.8 GHz, where the asymmetric T-junction lengths of L_{12} and L_{13} are selected such that $L_{13} - L_{12} = \lambda_{gl}/4$ to enable a balanced feed to the CPS (where λ_{gl} represents the wavelength at 1.8 GHz). The mitered bends in the asymmetric T-junction are used to minimize the signal variation in terms of magnitude and phase when being fed towards the dipole.

To further explain the design principles of the balun, a series of simulations have been performed, and their results are shown in Figures 2, 3, and 4. Figure 2(a) shows a wideband balun which has the reflection coefficients of −16.7 dB and −32.3 dB at 1.8 and 2.6 GHz, respectively. The transmission coefficients (S_{21}, S_{31}) are nearly −3.1 and −4.2 dB throughout the two bands which prove that the balun provides sufficient power to the CPS. However, the phase difference between ports 2 and 3 is observed to be 183.7° and 249.4° at 1.8 and 2.6 GHz, respectively. This implies that the differential

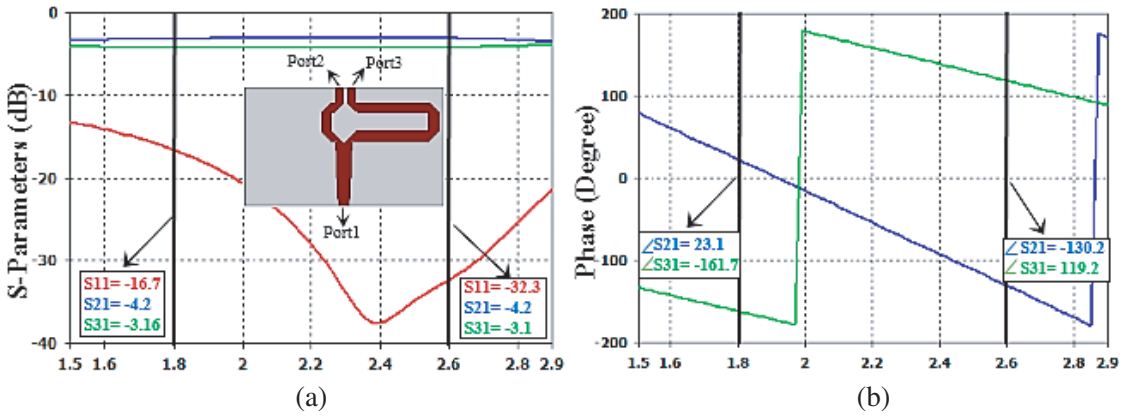

Figure 2. Independent simulation of the proposed balun, (a) S-parameters and (b) phase.

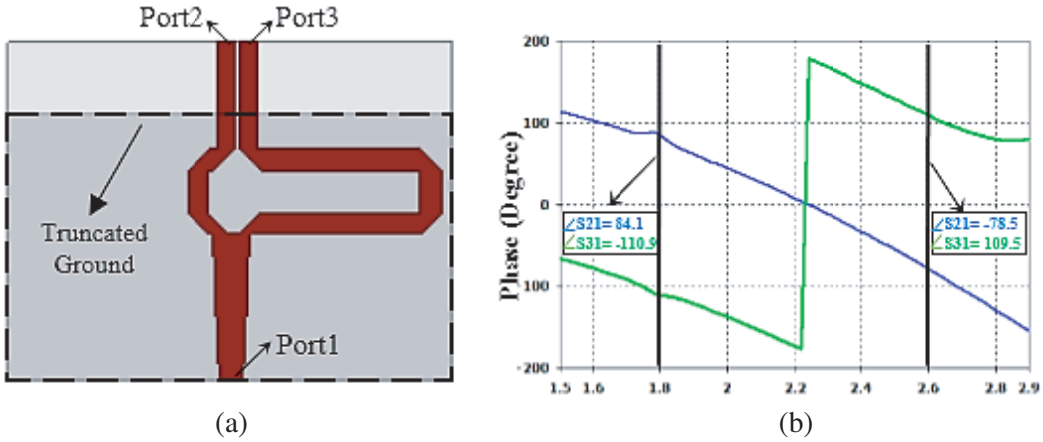

Figure 3. Simulation of balun, (a) balun with extended CPS line and (b) phase.

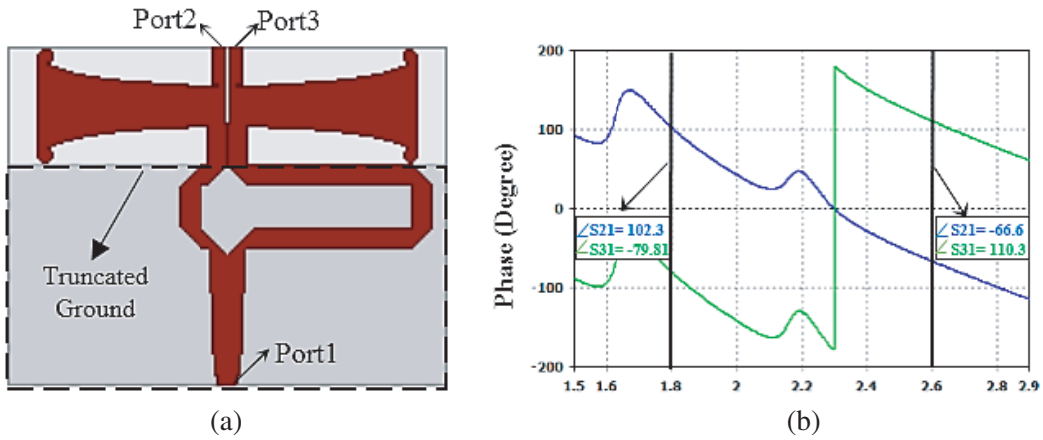

Figure 4. Independent simulation of the proposed balun, (a) balun with driven elements and (b) phase.

power can be delivered to the dipole at only 1.8 GHz, but not at 2.6 GHz. When the length of the CPS is increased while the truncated ground plane is kept constant, an out-of-phase behaviour is observed at both frequencies between ports 2 and 3, as shown in Figure 3. It can be seen that the CPS now transmits the differential power at both the frequencies. The final validation of ports 2 and 3 in terms of phase difference at the two frequencies in the presence of elliptical dipole is shown in Figure 4. It indicates that the differential power at ports 2 and 3 at 2.6 GHz is unaffected by the elliptical driver, thus another J-shaped driver can be placed in front of the elliptical driver to radiate efficiently at 2.6 GHz, as shown in Figure 1.

The microstrip-to-CPS transition is considered in this design, despite that a simpler differential CPS structure can be used to feed the antenna to reduce the size. Antennas fed using CPS typically degrades the antenna performance, because higher order modes are generated [30]. These extra modes may be beneficial in increasing the antenna's bandwidth, but at the same time, also results in degradation of gain in the intended operational bands. To ensure compactness, we have further optimized this design by enabling very close (but optimal) spacing between ground plane, two types of drivers, and director in the end-fire direction, relative to available literature [12, 14, 15, 17, 20]. On the other hand, the microstrip-to-CPS transition will provide differential output at the two dipoles with maximum power. In this design, the size of the CPS is kept small to ensure minimum generation of the additional higher order modes and provide differential feeding for dual-band operation. This is performed with care, ensuring minimal effects on the overall resulting phase from the CPS. This is to ensure that the proposed final structure is compact, with the close placement of the elliptical and J-shaped drivers to the output of the asymmetric T-junction. If the CPS is extended further while keeping the ground plane size constant, it is expected to affect the resulting phase negatively, which then tilts the main beam towards large angles off the end-fire direction. This will be explained further in Section 3.

The operation of the antenna is mainly enabled by the two types of driven elements, elliptical-shaped and J-shaped elements. The longer element is aimed in enabling operation in the lower band (from 1710 to 1880 MHz), and the shorter element is to enable operation in the higher band (from 2500 to 2700 MHz), as shown in Figure 1. To complement this explanation, a transmission line model shown in Figure 5 is also used to explain the concept of radiation mechanism. There are two parallel RLC series circuit element, each representing the pair of driven dipoles. Specifically, in Figure 5(a) the series RLC circuit on the left (representing the elliptical driver) resonates in LTE band 3 (centered at 1800 MHz) whereas the series RLC circuit on the right (representing the J-shaped driver) simultaneously acts as an open circuit. Similarly, for LTE band 7 (centered at 2600 MHz) the series RLC circuit on the right resonates while the circuit on the left is open, as shown in Figure 5(b).

Thus, the pair of dipoles is excited at different frequencies as half wave dipoles, with the non-excited element functioning as a reflector or director, depending on their lengths. This behavior enhances the directivity and gain of the antenna [26–28]. In the lower band, the ground acts as a reflector for the elliptical driver, and at the same time, the J-shaped driver acts as a director for the longer element.

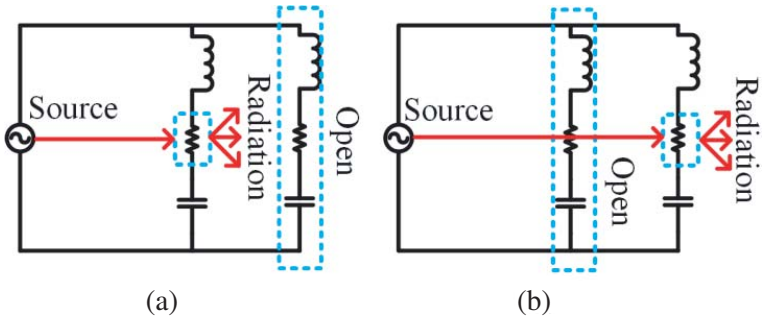

Figure 5. Transmission line model for radiation (a) at 1.8 GHz, and (b) at 2.6 GHz.

This phenomena causes the increase in the directivity in the lower band in the end fire direction. In the higher band, not only the ground but also elliptical driver support reflection in the higher band. In addition to it, the trapezoidal-shaped parasitic element acts as a director placed just in front of the J-shaped dipoles resulting in increased gain and directivity in the higher band. As this director is located closer to the J-shaped driver, the performance of the upper band is significantly affected in terms of reflection coefficient and gain in comparison with the lower band. Parametric study in Section 3, further explains the effect of reflectors and director in terms of radiation pattern and matching.

The lengths of the driven elements are chosen to be $\lambda_g/4$ at their resonance, with λ_g representing the guided wavelength. The elliptical dipole operates in the lower band with a major radius of 4.4 mm and a major-to-minor axis ratio of 5.1. Its edges are rounded-off with circular structures with the radius of 1.03 mm. The elliptical shape and rounded off edges cause the increase of the current path at lower resonant frequency [29]. The optimized dimensions of the proposed antenna are given in Table 2.

Table 2. Optimized dimensions of the proposed antenna.

Variable	Value (mm)	Variable	Value (mm)	Variable	Value (mm)
L_S	63	L_{11}	5.07	H_7	1.65
L_1	31	L_{12}	5.35	H_8	14.1
L_2	25	L_{13}	27.93	H_9	6.208
L_3	32.5	L_{14}	3.6	H_{10}	5.5
L_4	22.5	L_{15}	2.9	H_{11}	7.1
L_5	2	H_1	8	H_{12}	8.9
L_6	4.1	H_2	6	H_{13}	19.45
L_7	3.2	H_3	2	H_S	67
L_8	5.3	H_4	5.7	H_G	31.5
L_9	21.25	H_5	7.55	G_1	0.5
L_{10}	2.9	H_6	3	G_2	0.3

3. PARAMETRIC STUDY

To understand the effects of different parameters on the antenna bandwidth and radiation pattern, a series of parametric analysis is conducted. Parameters deemed to significantly influence its general performance include its ground plane height (H_G), the shape of the director, and the lengths of director (L_1 and L_2).

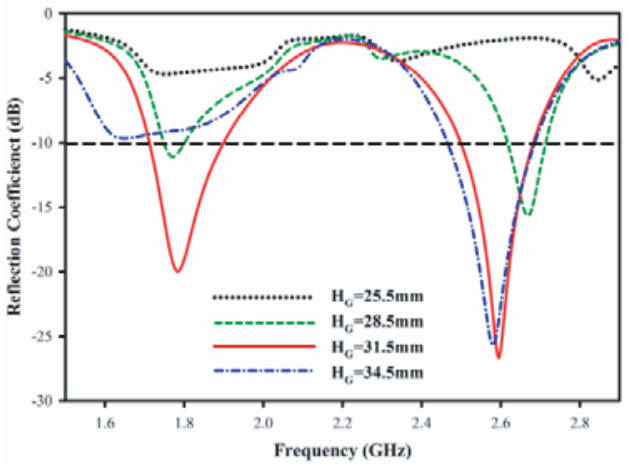

Figure 6. Effect of the ground height (H_G) on reflection coefficient.

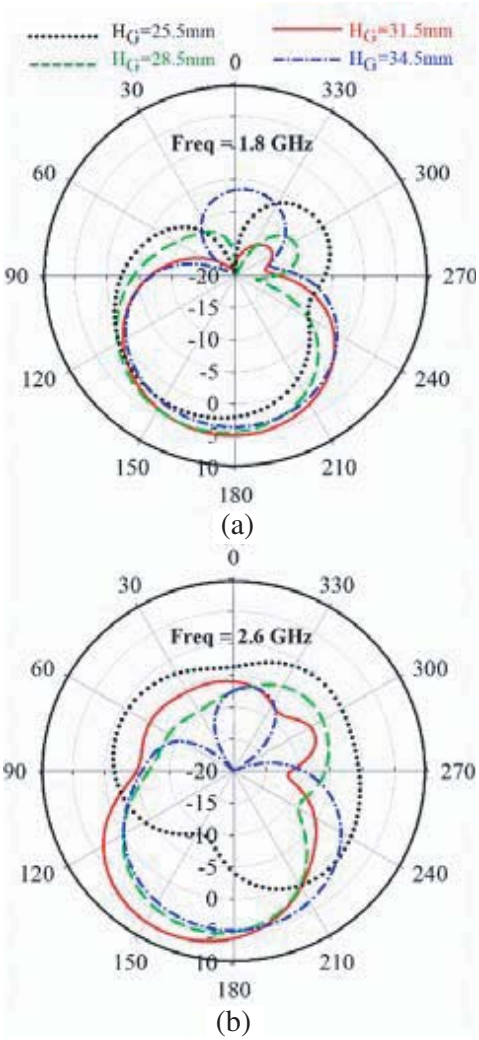

Figure 7. Effect of ground height H_G on radiation patterns at 1.8 GHz, and (b) at 2.6 GHz.

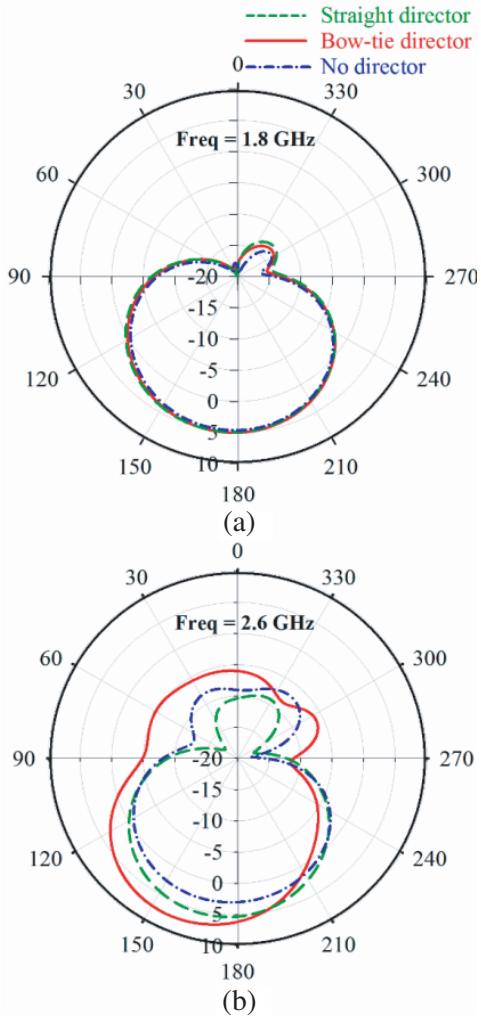

Figure 8. Effect of modifying the shape of director on radiation pattern in the azimuthal plane at (a) 1.8 GHz, and (b) at 2.6 GHz.

3.1. Effect of the Ground Plane Height (H_G)

The effects of the ground plane height H_G on the reflection coefficient and radiation pattern of the proposed antenna are shown in Figures 6 and 7, respectively. It can be observed that the antenna bandwidth is affected by changes in H_G. This section of the antenna facilitates matching in both its operating bands as shown in Figure 6. Besides that, H_G also affects the antenna gain in the end-fire direction, as shown in Figure 7. The main beam is slightly tilted due to the asymmetrical microstrip-to-CPS transition and the finite ground plane. The effect of microstrip-to-CPS transition can be overcome by increasing the size of ground plane. The main beam shifts towards the exact end-fire direction as H_G is increased. An optimal value of $H_G = 31.5$ mm is chosen to minimize the tilt in the end-fire and maximize gain in both bands. The ground width L_s also affects the gain in endfire direction which is not shown for brevity.

3.2. Effect of Modifying the Shape of Director

The gain improvement when employing different shapes of director is investigated: in the absence of directors and by replacing the straight director with a trapezoidal-shaped director. Figure 8 indicates that the gain in the lower band remains unaffected, with a minor increase from 0.2 to 0.3 dB when a trapezoidal-shaped director is used in the place of the straight director. On the contrary, the gain is significantly improved in the upper band when a trapezoidal-shaped director is used, as shown in Figure 8(b). This results in a gain of 7.3 dB 20° from the end-fire direction, and this degrades by 2 dB when a straight director is employed.

3.3. Effect of the Lengths of Director (L_1 and L_2)

The changes in terms of reflection coefficient due to the variations of the director lengths (L_1 and L_2) are illustrated in Figure 9. It is shown that these parameters are crucial in impedance matching. Changes in L_1 and L_2 significantly affect the matching in the upper band. On the contrary, the effects of these two parameters are not significant in the lower band. The lengths L_1 and L_2 are chosen to be 31 mm and 25 mm, respectively for better matching.

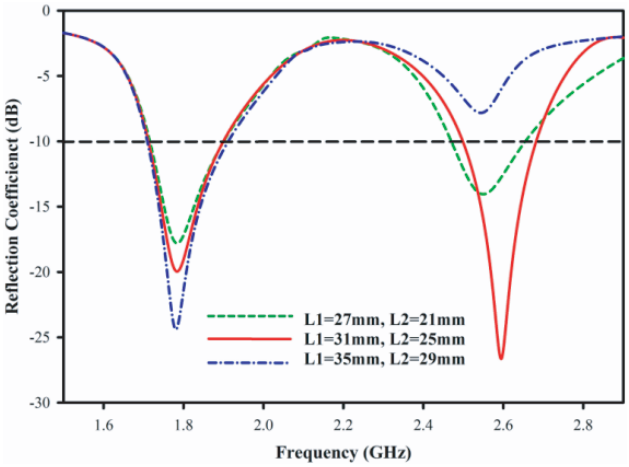

Figure 9. Effect of the lengths of director on reflection coefficient.

From Figures 8 and 9, it is concluded that the gain as well as reflection coefficient in the upper band is more prone to the changes in the shape and length of the director compared to the lower band. This is due to the direct coupling of the director with the J-shaped dipole and contrary to the dipole configuration in the lower band.

It can be summarized from the parametric study that high antenna gains can be achieved in both bands by choosing an appropriate shape of the drivers, director and the ground. Besides that, the

Table 3. Summary of the parametric study on the gain of antenna.

Parameters	Length (mm)	Gain (dB) Band 1	Gain (dB) Band 2
H_G	25.5	3.2	2
	28.5	4.8	6.5
	31.5	5.2	7.4
	34.5	4.1	5.12
Effect of the director shape on gain			
No director		4.62	3.14
Straight director		4.97	5.5
Trapezoidal director		5.02	7.4

gain in the upper band also varies significantly compared to the lower band. It is due to the use of the elliptical-shaped driver that acts as a good reflector for the J-shaped driver. The results of the parametric study are summarized in Table 3.

4. RESULTS AND DISCUSSION

The antenna is designed and optimized using the commercial electromagnetic solver HFSS, which is based on the finite element method (FEM).

4.1. Current Distribution

Figure 10 illustrates the simulated current distributions of the antenna at the centre frequencies and the fabricated prototype. It can be seen that the current on the elliptical-shaped radiating element is intense in the lower band. The same can be observed for the currents on the J-shaped radiator when being simulated in the upper band. The director which excites radiation towards the end-fire direction indicates high current intensity in the upper band as compared to the lower band. Thus, it can be concluded that the upper frequency band is more sensitive to the design and position of the director.

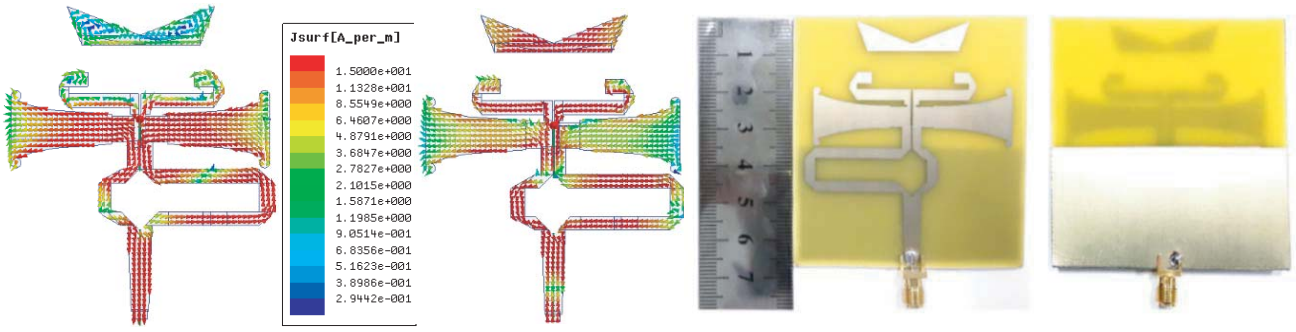

(a) (b) (c)

Figure 10. Simulated current distribution of the antenna and its fabricated prototype showing (a) simulated current distribution at 1.8 GHz, (b) simulated current distribution at 2.6 GHz, and (c) top and bottom view of fabricated prototype.

4.2. Reflection Coefficient, Gain and Efficiency

Figure 11 presents the simulated and measured reflection coefficients, gains, and efficiencies. It can be seen that the 10 dB impedance bandwidth of the proposed antenna ranges from 1.71 to 1.9 GHz and 2.5

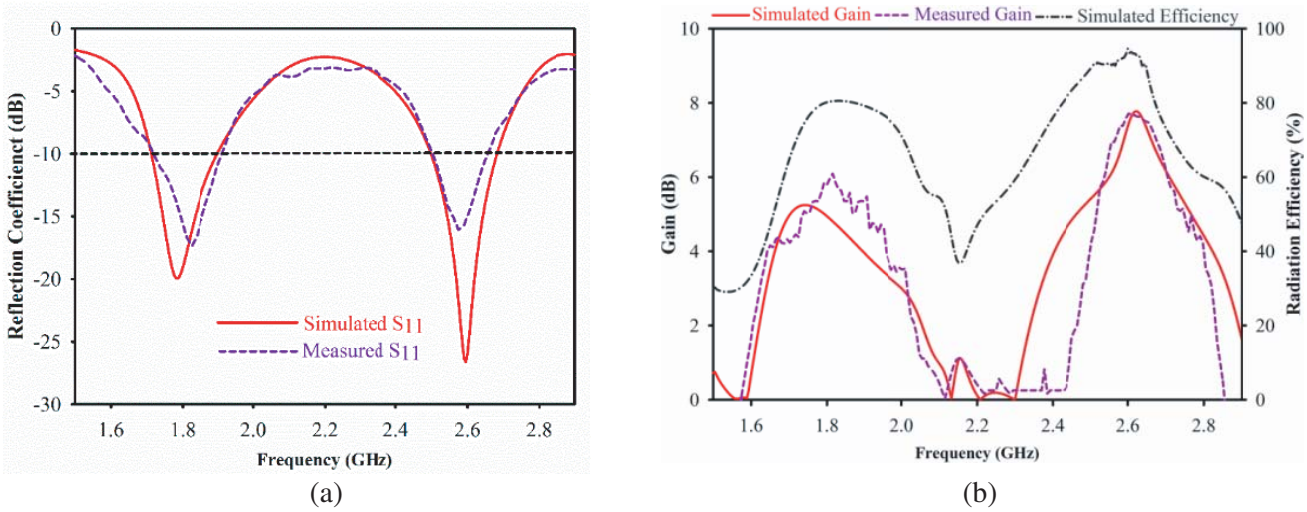

Figure 11. Simulated and measured performance in term of (a) reflection coefficient, and (b) gain and efficiency.

to 2.7 GHz, covering LTE band 3 and band 7. Its corresponding fractional bandwidth is about 10.5% (in the lower band) and 4% (in the upper band). There is good agreement between the simulated and measured results shown in Figure 11(a), with a small discrepancy which can be attributed to the SMA connector used to feed the fabricated antenna. Figure 11(b) illustrates the simulated and measured gains from 1.5 to 2.9 GHz. The measured antenna gain ranges from 4.3 to 6 dB in lower band and from 3.7 to 7.7 dB in the upper band. The peak measured gain is found to be 6 dB at 1.815 GHz in lower band and 7.7 dB at 2.623 GHz in the upper band. The simulated efficiencies at these frequencies are 80% and 94%, respectively.

4.3. Radiation Pattern

Figure 12 illustrates the simulated and measured radiation patterns at 1.8 and 2.6 GHz. It is shown that the cross-polarization is at least −12 dB lower than the co-polarized fields in the peak gain direction. The peak gain is directed 10° off the end-fire axis in the lower band and 20° in the upper band. From

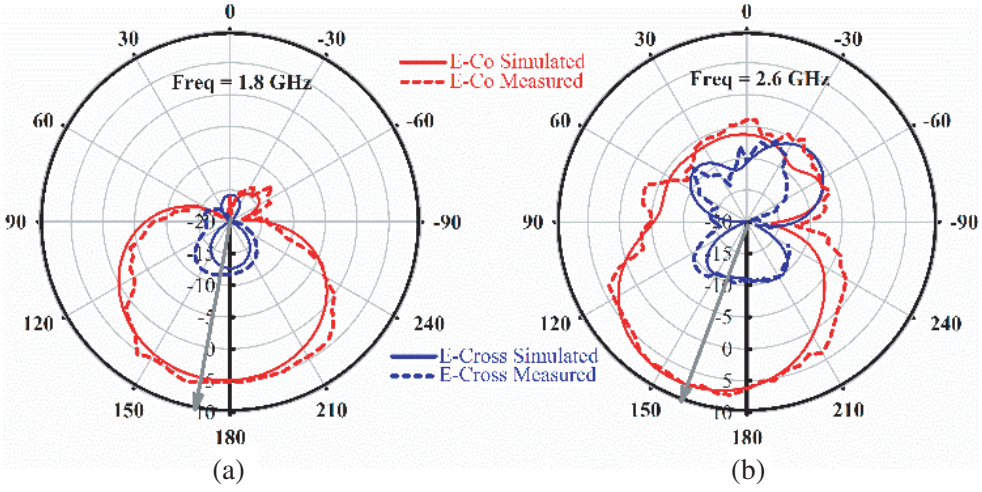

Figure 12. Simulated and measured performance in term of Radiation pattern showing (a) at 1.8 GHz, and (b) at 2.6 GHz.

the co- and cross-polarized fields, it is concluded that the antenna is linearly polarized, which is suitable for MIMO applications as in [31].

5. CONCLUSION

A high gain, dual-band quasi Yagi antenna is designed for LTE applications. A set of closely-spaced driven elements and director are employed to improve the gain and directivity of antenna. The simulated and measured results are in good agreement with each other, with fractional bandwidths of 10.5% (in the lower band) and 4% (in the upper band) for LTE band 3 and band 7, respectively. The proposed antenna produces a peak gain of 6 dB in the lower band and 7.7 dB in the upper band. Radiation patterns indicate that the antenna is linearly polarized, with a satisfactory level of polarization discrimination. Radiation is found to be directed slightly off the end-fire direction.

REFERENCES

1. Holma, H., A. Toskala, K. Ranta-Aho, and J. Pirskanen, "High-speed packet access evolution in 3GPP release 7 [Topics in radio communications]," *IEEE Communications Magazine*, Vol. 45, No. 12, 29–35, 2007.
2. Mun, B., F. J. Harackiewicz, B. Kim, H. Wi, J. Lee, M. J. Park, and B. Lee, "New configuration of handset MIMO antenna for LTE 700 band applications," *International Journal of Antennas and Propagation*, Vol. 2013, 6 pages, 2013.
3. Dadgarpour, A., B. Zarghooni, B. S. Virdee, and T. A. Denidni, "Millimeter-wave high-gain SIW end-fire bow-tie antenna," *IEEE Transactions on Antennas and Propagation*, Vol. 63, No. 5, 2337–2342, 2015.
4. Sun, M., X. Qing, and Z. N. Chen, "60-GHz end-fire fan-like antennas with wide beamwidth," *IEEE Transactions on Antennas and Propagation*, Vol. 61, No. 4, 1616–1622, 2013.
5. Pazin, L. and Y. Leviatan, "A compact 60-GHz tapered slot antenna printed on LCP substrate for WPAN applications," *IEEE Antennas and Wireless Propagation Letters*, Vol. 9, 272–275, 2010.
6. Shao, J., G. Fang, Y. Ji, K. Tan, and H. Yin, "A novel compact tapered-slot antenna for GPR applications," *IEEE Antennas and Wireless Propagation Letters*, Vol. 12, 972–975, 2013.
7. Nikolic, N. and A. R. Weily, "Compact E-band planar quasi-Yagi antenna with folded dipole driver," *IET Microwaves, Antennas & Propagation*, Vol. 4, No. 11, 1728–1734, 2010.
8. Wu, J., Z. Zhao, Z. Nie, and Q. H. Liu, "Bandwidth enhancement of a planar printed quasi-Yagi antenna with size reduction," *IEEE Transactions on Antennas and Propagation*, Vol. 62, No. 1, 463–467, 2014.
9. Qin, P. Y., A. R. Weily, Y. J. Guo, T. S. Bird, and C. H. Liang, "Frequency reconfigurable quasi-Yagi folded dipole antenna," *IEEE Transactions on Antennas and Propagation*, Vol. 58, No. 8, 2742–2747, 2010.
10. Liu, J. and Q. Xue, "Microstrip magnetic dipole Yagi array antenna with endfire radiation and vertical polarization," *IEEE Transactions on Antennas and Propagation*, Vol. 61, No. 3, 1140–1147, 2013.
11. Cai, R.-N., S. Lin, G.-L. Huang, X.-Y. Zhang, X.-Q. Zhang, W.-B. Zhang, and J.-X. Wang, "Research on a novel Yagi-Uda antenna fed by balanced microstrip line," *IEEE China-Japan Joint Microwave Conference Proceedings (CJMW)*, 1–4, 2011.
12. Zong, H., H. Gu, H. Li, B. Liu, G. Liu, and Q. Wu, "A novel high-gain quasi-Yagi antenna with a parabolic reflector," *2015 International Symposium IEEE Antennas and Propagation (ISAP)*, 1–3, 2015.
13. Farran, M., D. Modotto, S. Boscolo, A. Locatelli, A. D. Capobianco, M. Midrio, and V. Ferrari, "Microstrip-fed quasi-Yagi antennas for WLAN applications," *2014 11th IEEE European Radar Conference (EuRAD)*, 384–387, 2014.
14. Kim, D. O. and C. Y. Kim, "Dual-band quasi-Yagi antenna with split ring resonator directors," *Electronics Letters*, Vol. 48, No. 14, 809–810, 2012.

15. Steyn, J. M., J. W. Odendaal, and J. Joubert, "Double dipole antenna for dual-band wireless local area networks applications," *Microwave and Optical Technology Letters*, Vol. 51, No. 9, 2034–2038, 2009.
16. Jehangir, S. S. and M. S. Sharawi, "A miniaturized dual wide-band loop excited quasi-yagi antenna using a defected ground structure," *IEEE 2016 16th Mediterranean Microwave Symposium (MMS)*, 1–3, 2016.
17. Zhang, Y. and Z. Li, "A dual-band planar quasi-Yagi antenna with double-dipole driver," *IEEE 6th International Symposium on Microwave, Antenna, Propagation, and EMC Technologies (MAPE)*, 123–125, 2015.
18. Cheong, P., K. Wu, W. W. Choi, and K. W. Tam, "Yagi-Uda antenna for multiband radar applications," *IEEE Antennas and Wireless Propagation Letters*, Vol. 13, 1065–1068, 2014.
19. Ding, Y., Y. C. Jiao, P. Fei, B. Li, and Q. T. Zhang, "Design of a multiband quasi-Yagi-type antenna with CPW-to-CPS transition," *IEEE Antennas and Wireless Propagation Letters*, Vol. 10, 1120–1123, 2011.
20. Khan, O. M., Z. U. Islam, Q. U. Islam, and F. A. Bhatti, "Multiband high-gain printed Yagi array using square spiral ring metamaterial structures for S-band applications," *IEEE Antennas and Wireless Propagation Letters*, Vol. 13, 1100–1103, 2014.
21. Wu, S. J., C. H. Kang, K. H. Chen, and J. H. Tarng, "A multiband quasi-Yagi type antenna," *IEEE Transactions on Antennas and Propagation*, Vol. 58, No. 2, 593–596, 2010.
22. Qian, Y. and T. Itoh, "A broadband uniplanar microstrip-to-CPS transition," *1997 Asia-Pacific Microwave Conference Proceedings, APMC'97*, 609–612, 1997.
23. Han, K. H., B. Lacroix, J. Papapolymerou, and M. Swaminathan, "New microstrip-to-CPS transition for millimeter-wave application," *2011 IEEE 61st Electronic Components and Technology Conference (ECTC)*, 1052–1057, 2011.
24. Rizzi, P. A., *Microwave Engineering: Passive Circuits*, Prentice Hall, 1988.
25. Mongia, R. K., J. Hong, P. Bhartia, and I. J. Bahl, *RF and Microwave Coupled-line Circuits*, Artech House, 2007.
26. Eldek, A. A., "Design of double dipole antenna with enhanced usable bandwidth for wideband phased array applications," *Progress In Electromagnetics Research*, Vol. 59, 1–15, 2006.
27. Ta, S. X., J. J. Han, H. Choo, and I. Park, "A wideband double dipole quasi-Yagi antenna using a microstrip-slotline transition feed," *IEEE International Workshop on Antenna Technology (iWAT)*, 84–87, 2012.
28. Chang, D. C., C. B. Chang, and J. C. Liu, "Modified planar quasi-Yagi antenna for WLAN dual-band operations," *Microwave and Optical Technology Letters*, Vol. 46, No. 5, 443–446, 2005.
29. Berge, L. A., M. T. Reich, and B. D. Braaten, "A compact dual-band bow-tie slot antenna for 900-MHz and 2400-MHz ISM bands," *IEEE Antennas and Wireless Propagation Letters*, Vol. 10, 1385–1388, 2011.
30. Zhu, L. and K. Wu, "Field-extracted lumped-element models of coplanar stripline circuits and discontinuities for accurate radiofrequency design and optimization," *IEEE Transactions on Microwave Theory and Techniques*, Vol. 50, No. 4, 1207–1215, 2002.
31. Jehangir, S. S. and M. S. Sharawi, "A miniaturized dual UWB quasi-Yagi based MIMO antenna system using a defected ground structure," *2018 IEEE International Symposium on Antennas and Propagation & USNC/URSI National Radio Science Meeting*, 399–400, Boston, MA, 2018.